JOURNAL OF GEOPHYSICAL RESEARCH, VOL. ???, XXXX, DOI:10.1029/,

Pulse-like, crack-like, and supershear earthquake ruptures with shear strain localization

Eric G. Daub,[1] M. Lisa Manning,[2] and Jean M. Carlson[1]

Abstract. We incorporate shear strain localization into spontaneous elastodynamic rupture simulations using a Shear Transformation Zone (STZ) friction law. In the STZ model, plastic strain in the granular fault gouge occurs in local regions called STZs. The number density of STZs is governed by an effective disorder temperature, and regions with elevated effective temperature have an increased strain rate. STZ Theory resolves the dynamic evolution of the effective temperature across the width of the fault zone. Shear bands spontaneously form in the model due to feedbacks amplifying heterogeneities in the initial effective temperature. In dynamic earthquake simulations, strain localization is a mechanism for dynamic fault weakening. A shear band dynamically forms, reduces the sliding stress, and decreases the frictional energy dissipation on the fault. We investigate the effect of the dynamic weakening due to localization in generating pulse-like, crack-like, and supershear rupture. Our results illustrate that the additional weakening and reduction of on-fault energy dissipation due to localization have a significant impact on the initial shear stress required for supershear or pulse-like rupture to propagate on a fault.

1. Introduction

The earthquake rupture problem spans a wide range of length and time scales, from microscopic contacts between individual grains through complex networks of faults. The basic interactions at the smallest scales form the basis for larger scale behavior. Modeling earthquake rupture is therefore extremely challenging, as models must capture the essential physics at a given scale and determine how larger scales will be affected by the smaller scale physics.

Constitutive laws play a central role in investigating the complexity of seismicity. This includes spatiotemporal complexity [e.g., *Carlson and Langer*, 1989; *Cochard and Madariaga*, 1996; *Shaw and Rice*, 2000], and the complexity of individual ruptures [e.g., *Perrin et al.*, 1995; *Zheng and Rice*, 1998; *Nielsen et al.*, 2000; *Bizzarri and Cocco*, 2005]. Because the friction law is usually the only ingredient in an earthquake model that accounts for small scale physics, developing constitutive laws that efficiently incorporate physical processes is essential for improving our understanding of the physics of the earthquake source.

This work focuses on the implications of a constitutive law that accounts for the small scale process of strain localization in the granular fault cores of earthquake faults. In our model, a shear band that is narrow even on the scale of the fault gouge spontaneously forms due to fault slip. Localization of strain is observed in many studies of faulting, including numerical simulations [*Morgan and Boettcher*, 1999], laboratory experiments [*Marone*, 1998], and field observations of exhumed faults [*Chester and Chester*, 1998]. The prevalance of shear bands in many studies indicates that localization widely affects faults.

Constitutive laws used in dynamic rupture models usually do not explicitly account for localization. Traditionally, dynamic rupture is modeled on a planar fault with a slip-weakening [*Ida*, 1972; *Andrews*, 1976] or rate and state friction law [*Dieterich*, 1979; Ruina, 1980], where the fault strength depends only on a single state variable. We include localization in our modeling by resolving the dynamic evolution of the strain rate on a spatial grid that spans the width of the fault core. In our model, the fault dynamically selects how to distribute strain within the fault core, and can accomodate both broad and localized shear within the slip history of a single earthquake. This approach allows us to investigate the fault scale consequences of the dynamics of shear localization.

This work is part of our efforts to develop the first steps in a physical description of the frictional properties of fault gouge and connects small scale physics to fault scale dynamics. Because the small scale physics of earthquake rupture are poorly constrained, seismologists do not know exactly how fault gouge deforms during earthquake slip. However, fault gouge is composed of particles of a large range of diameters that do not form a regular crystal structure [*Chester et al.*, 2005], making it an amorphous material. Therefore, we turn to the physics of amorphous materials for our constitutive law for earthquake rupture. Physicists have shown that there are similarities in the deformation of a wide range of amorphous materials [e.g. *Falk and Langer*, 1998, 2000; *Ono et al*, 2002; *Lois et al.*, 2005], and these common features are independent of the details of the small scale interactions between particles. Because of this, we use a friction law based on Shear Transformation Zone (STZ) Theory [*Falk and Langer*, 1998, 2000], which captures these common features of plastic deformation.

This study builds upon our initial work using STZ Theory to resolve strain localization in dynamic rupture simulations [*Daub et al.*, 2008]. STZ Theory ties fault weakening to the evolution of an effective temperature that quantifies the configurational disorder in the granular fault gouge [*Langer*, 2008]. In our previous work, fault slip sponatenously formed a shear band of a fixed width in the fault gouge during dynamic rupture simulations, and we compared the propagation of dynamic ruptures with and without shear band formation. This simplified approach captured the basic physics of strain localization, but the rupture calculations did not include diffusion of the effective temperature. In this study, we expand upon our initial studies and include the full diffusion

[1]Physics Department, University of California, Santa Barbara, California, USA

[2]Princeton Center for Theoretical Science, Princeton University, Princeton, New Jersey, USA

Copyright 2009 by the American Geophysical Union.
0148-0227/09/$9.00

equation for the effective temperature in an elastodynamic rupture simulation. This approach allows for a balance between the dynamic processes of energy dissipation and diffusion to select the width of shear bands in our rupture simulations, and we explore the fault scale consequences of strain localization. Additionally, we add a relaxation term to the STZ law, which incorporates time-dependent healing and allows for self-healing pulse-like ruptures to propagate in dynamic rupture simulations.

We begin with a brief overview of the STZ friction law, and follow that with a discussion of its implications for fault friction. We then look to the larger scale of dynamic fault rupture, and investigate the implications of shear bands in numerical simulations of earthquakes.

2. STZ Friction Law

At the scale of fault gouge, we model friction with STZ Theory, a continuum approximation for plastic deformation in dense amorphous solids. STZ Theory has been applied to a wide variety of systems, including fracture of glassy materials [*Falk and Langer*, 1998, 2000], boundary lubrication [*Lemaitre and Carlson*, 2004], granular flow [*Lois et al.*, 2005], and dynamic earthquake rupture [*Daub and Carlson*, 2008]. Recent studies with STZ Theory described the dynamics of shear banding in glassy materials [*Manning et al.*, 2007; *Manning et al.*, 2009] and in earthquake faults [*Daub et al.*, 2008]. A full derivation of the equations of STZ Theory can be found in Appendix A. Here, we provide a brief summary to physically motivate the theory.

An illustration of the range of scales in the earthquake problem is shown in Figure 1. The fault consists of a layer of gouge sheared between elastic rock (left in Figure 1). Within the layer of fault gouge, deformation tends to spontaneously localize into narrow shear bands, as shown in the center picture in Figure 1. At the grain scale, the gouge deforms plastically when groups of particles rearrange (right, Figure 1). The STZ model captures the plastic deformation at the grain and gouge scales, and also acts as a friction law that describes fault scale behavior in elastodynamic rupture simulations.

The deformation of an amorphous solid can be approximated by two components – affine displacements, where all of the individual particle displacements are consistent with uniform elastic strain in the material, and non-affine displacements, where the individual particle motions are heterogeneous and vary from particle to particle. Non-affine deformation is calculated by subtracting the particle displacements consistent with uniform elastic strain from the total particle displacements. Affine deformation results in a purely elastic material response. Simulations show that non-affine deformation can be either elastic or plastic, but STZ Theory make the simplifying assumption that non-affine displacements result in purely plastic deformation. Simulations of sheared amorphous materials indicate that the non-affine displacements tend to occur in small, localized regions, called Shear Transformation Zones (STZs) [*Falk and Langer*, 1998, 2000]. The simulations find that these STZs constitute a small collection of particles switching between two metastable orientations under applied shear stress.

The STZ friction model incorporates the microscopic observations of non-affine particle displacements by assuming that all plastic deformation occurs through STZ rearrangements. Each reversal from one orientation to the other accumulates a certain amount of plastic strain, and a threshold shear stress must be applied for the reversal to occur. STZ Theory treats the populations of the two STZ orientations as dynamic state variables. STZs can flip from one orientation to the other, and are created and destroyed as the system is sheared. Creation and annihilation drive the number density of STZs towards a Boltzmann distribution, with an effective temperature χ. The effective temperature describes the configurational disorder in the material. Regions that have a higher effective temperature are more disordered, have a higher density of STZs, and accomodate more plastic strain. Effective temperature has been measured in simulations [*Ono et al.*, 2002] and experiments [*Schröter et al.*, 2005] for various amorphous materials.

In fault materials, the effective temperature describes the disorder in the gouge packing, which determines the internal state of the material. The disorder due to the many ways to pack the material is much more significant than the disorder due to thermal fluctuations for fault materials. Even at seismogenic depths, thermal fluctuations are not large enough to drive rearrangements in the material. The energy to form an STZ must therefore come from external shearing of the material, which alters the gouge packing and changes the effective temperature. Therefore, the evolution of the effective temperature determines the dynamics of friction. The thermal temperature can still have an effect on friction, as material properties vary with the thermal temperature, though it does not enter directly into the constitutive equations.

Quantitatively, the total rate of shear deformation D_{ij}^{tot} can be written as the sum of elastic and plastic components. STZ theory determines the plastic shear strain rate $\dot{\gamma}$ in the material based on two factors: the effective temperature, which determines the number of STZs, and the shear stress τ, which determines how frequently the STZs switch orientation. We summarize these two contributions as follows:

$$\dot{\gamma} = f(\tau) \exp(-1/\chi) . \tag{1}$$

The function $f(\tau)$ describes how the STZ reversals depend on the shear stress, and also incoporates a yield stress τ_y, below which the plastic strain rate is zero and the fault locks. If the stress is below the yield stress, $f(\tau) = 0$ and no plastic deformation occurs. Although the constitutive equations allow for the fault to truly lock, we find that in practice, the plastic strain rate never falls to zero during dynamic rupture simulations. If the stress is above the yield stress, $f(\tau) = (2\epsilon/t_0)\exp(-E_0)\cosh(\tau/\sigma_d)(1-\tau_y/\tau)$, the details of which are discussed in Appendix A. The parameter meanings and values of are summarized in Table 1. For the large values of shear stress in seismic faulting, $f(\tau) \approx \exp(-E_0 + \tau/\sigma_d)$, which produces the logarithmic rate dependence observed in rock mechanics experiments [*Dieterich*, 1979]. However, materials other than fault gouge may have different forms for $f(\tau)$.

Table 1. Parameter descriptions and their values in the STZ model.

Parameter	Description
$t_0 = 0.000001$ s	STZ rearrangement time scale
$\epsilon = 10$	Strain increment for STZ rearrangement
$E_0 = 40$	STZ activation energy scaled by STZ formation energy
$\sigma_d = 0.5$ MPa	STZ activation stress (also known as the direct effect stress)
$\tau_y = 25$ MPa	STZ yield stress
$c_0 = 400$	Effective temperature specific heat
$\chi_w = 0.2$	Effective temperature activation barrier
$q_0 = 0.08$	Nondimensional strain rate ($\dot{\gamma}t_0$) where STZ Theory breaks down
$R_0 = 5$ s^{-1}	Inverse of STZ relaxation time scale
$\beta = 0.1$	STZ relaxation activation barrier
$\chi_0 = 0.007$	Lowest effective temperature that can be reached by relaxation
$D =$ varies	Squared diffusion length scale

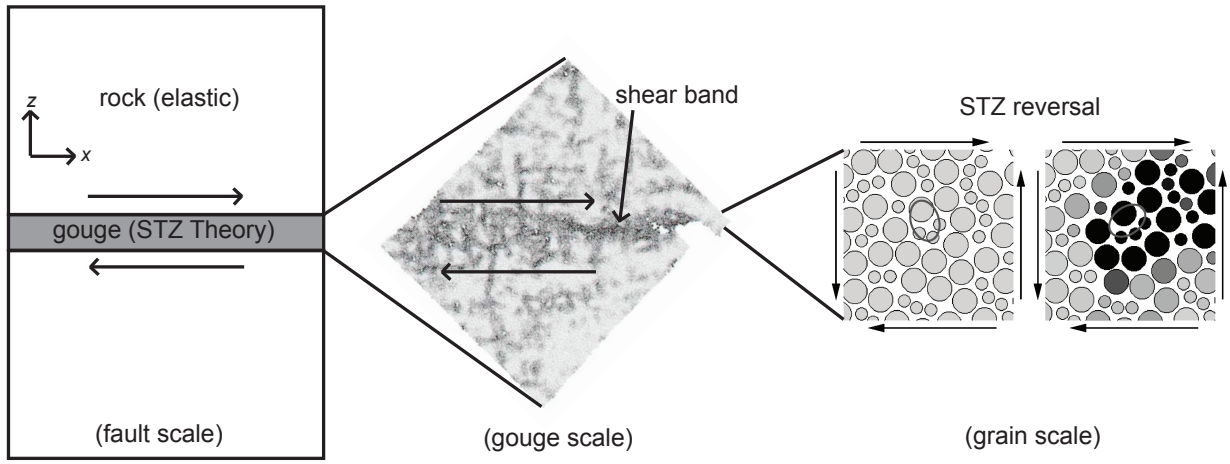

Figure 1. Diagram illustraing the multi-scale nature of the earthquake rupture problem. The system progressively decreases in scale from left to right. (left) Fault scale, with a thin layer of fault gouge sheared between elastic rocks. (center) Deformation within the fault gouge, where a shear band that is much narrower than the gouge thickness accomodates plastic strain in the gouge. Shear band image taken from *Falk and Shi* [2002] and reoriented to match the sense of shear of the fault and grains. (right) Individual rearrangements occur at the grain scale and produce plastic strain in the fault gouge. The left grain scale picture shows a "positive" STZ orientation, and as the grains are sheared the gouge deforms plastically and the particles change to a "negative" orientation in the right grain picture. STZ diagram taken from *Falk and Langer* [1998].

The function $f(\tau)$ introduces two characteristic stresses – the yield stress τ_y, and the STZ activation stress σ_d. The yield stress is the minimum value of the macroscopic shear stress that must be applied for the system to deform plastically, as STZ Theory is a continuum approximation that assumes that the macroscopic shear stress is sufficient to describe the flipping of STZs. The values of both stress parameters are likely to be proportional to the normal stress, as an increase in the confining pressure makes STZ rearrangements less likely to occur and require a proportional increase in the applied shear stress to achieve the same plastic strain rate. This is consistent with rock mechanics experiments [*Dieterich*, 1979]. We only simulate 2D ruptures along strike, where the normal stress is constant, so we hold τ_y and σ_d constant. However, these parameters would vary in a system where normal stress is not constant.

In addition to the relation between strain rate, stress, and effective temperature (Equation (1)), the model requires a dynamic evolution equation for the effective temperature. We include terms for energy dissipation, diffusion, and time-dependent relaxation in the governing partial differential equation for the effective temperature:

$$\frac{\partial \chi}{\partial t} = \frac{\dot{\gamma}\tau}{c_0 \tau_y}\left(1 - \frac{\chi}{\hat{\chi}(\dot{\gamma})}\right) + \frac{\partial}{\partial z}\left(\dot{\gamma} D \frac{\partial \chi}{\partial z}\right) + R_0\left(1 - \frac{\chi}{\chi_0}\right)\exp\left(\beta/\chi\right). \quad (2)$$

As work is done on the material, the dissipation term drives the effective temperature towards a steady-state effective temperature $\hat{\chi}(\dot{\gamma})$ that depends on the strain rate [*Langer and Manning*, 2007]. As the strain rate in the material increases, the steady-state effective temperature rises. Only part of the dissipated energy increases the effective temperature in the material; the remainder increases the thermal temperature and leads to frictional heating of the gouge. Energy dissipation is an important topic in fault mechanics, and we more thoroughly investigate this problem in another study (A. M. Hermunstad, E. G. Daub, and J. M. Carlson, Energetics of strain localization in a model of seismic slip, submitted to *Journal of Geophysical Research*, 2009). Diffusion occurs with a time scale determined by the inverse strain rate and length scale $\sqrt{D}$. Diffusion of effective temperature is observed in simulations [*Shi et al.*, 2007], and only occurs if the material is being deformed. The healing term allows for time-dependent restrengthening on the fault, and relaxes the effective temperature towards the minimum

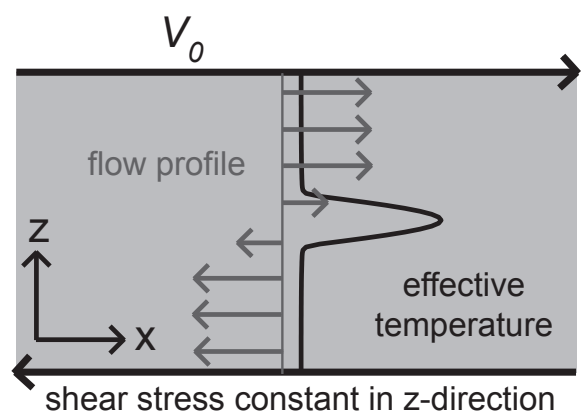

Figure 2. Diagram illustrating a layer of fault gouge driven at its boundary at a constant velocity V_0. We resolve the effective temperature dynamics as a function of position across the thickness of the gouge. This is illustrated by the black curve, which shows the effective temperature as a function of position in the gouge. Because the effective temperature evolves in space and time, the STZ model captures the dynamic evolution of the strain rate in the material, and the flow profile in the gouge, which is shown in gray in the illustration. Shear stress is assumed to evolve rapidly compared to the effective temperature, and is always spatially homogeneous.

value χ_0. Strength recovers logarithmically with time, as observed in laboratory experiments [*Dieterich*, 1972].

Our choice of $\hat{\chi}(\dot{\gamma})$ is based on the observed rate dependence of the steady-state effective temperature in a simulated glass [*Langer and Manning*, 2007]:

$$\hat{\chi}\left(\dot{\gamma}\right) = \frac{\chi_w}{\log\left(\frac{q_0}{t_0\dot{\gamma}}\right)}. \tag{3}$$

If the parameter χ_w is less than unity, the friction law weakens with increasing strain rate in steady state. The parameter q_0 determines the dimensionless strain rate at which the effective temperature diverges. At strain rates higher than q_0/t_0, the deformation is no longer accomodated as local STZs and instead as amorphous flow. The value of $q_0 = 0.08$ that we use is deduced from molecular dynamics simulations [*Haxton and Liu*, 2007]. Because the time scale for STZ rearrangement is very fast, our value of q_0 corresponds to a strain rate larger than the strain rate expected during seismic slip. This means that the constitutive equations are valid at the strain rates in our simulations.

STZ Theory introduces many parameters, which come from our aim to represent the underlying physics of gouge deformation simply but accurately, and not from simply fitting data in experiments. Parameters are needed to connect the small scale physics to the larger scale frictional behavior, and most of the parameters are constrained by simulations and experimental data. The resulting friction dynamics are generic for the theory and are robust to variations in the parameter values.

Because the governing equation for the effective temperature is a partial differential equation, the STZ model has many more degrees of freedom than single state variable laws such as Dieterich-Ruina friction. This allows for more complex behavior of macroscopic friction when the STZ model is applied to the larger scale problem of interfacial dynamics.

3. STZ Friction Dynamics

In this section, we look at the dynamics of friction when the STZ law is applied to a layer of fault gouge under shear. A schematic of the system is shown in Figure 2. A layer of gouge of width $2w$ is sheared from the boundary at a constant driving rate V_0. We assume that the shear stress is constant within the layer. This is because the time scale for stress equilibration (the width of the gouge divided by the speed of sound) is much smaller than the time scale for effective temperature evolution (the inverse plastic strain rate). Due to this difference in time scales, the stress is always spatially uniform in the z-direction, which is the static solution to the continuum momentum conservation equation in this geometry.

The xz component of the total rate of deformation tensor D_{xz}^{tot} is the sum of elastic and plastic parts:

$$\begin{aligned} D_{xz}^{tot} &= \frac{1}{2}\left(\frac{\partial v_x}{\partial z} + \frac{\partial v_z}{\partial x}\right) \\ &= \frac{\mathcal{D}}{\mathcal{D}t}\left(\frac{\tau_{xz}}{2\mu}\right) + \dot{\gamma}_{xz}, \end{aligned} \tag{4}$$

where $\mathcal{D}/\mathcal{D}t$ indicates a material or corotational derivative. In the case of simple shear with translational symmetry in the x-direction, the material derivative reduces to a partial derivative with respect to time, and the total rate of deformation is given by $(1/2)\partial v_x/\partial z$. Therefore, Equation 4 simplifies to

$$\frac{1}{2}\frac{\partial v_x}{\partial z} = \frac{1}{2\mu}\frac{d\tau}{dt} + \dot{\gamma}. \tag{5}$$

Here, we have dropped indices on the stress and strain rate, and since the stress is spatially uniform, changed the partial derivative with respect to time into a full derivative with respect to time.

If we integrate both sides of Equation 5 over the entire width of the material in the z-direction, we obtain the diferential equation describing stress evolution:

$$\frac{d\tau}{dt} = \frac{\mu}{w}\left(V_0 - \int_{-w}^{w} \dot{\gamma}\, dz\right). \tag{6}$$

Driving the system causes the stress to increase at a rate determined by the shear modulus μ, while plastic strain decreases the shear stress. Note that because the stress is constant across the width of the gouge, any localization of strain is due to spatial variations in the effective temperature (i.e. the configurational disorder in the gouge). Shear bands form because the disorder in the material becomes heterogeneous, and not because of spatial variations in the shear stress.

The equations for stress evolution (Equation (6)) and effective temperature evolution (Equation (2)) are integrated numerically to model the dynamics of friction in the layer. We use a typical seismic slip rate of $V_0 = 1$ m/s, a fault gouge width of $w = 0.1$ m based on a field study by *Chester and Chester* [1998], and a shear modulus of $\mu = 32$ GPa. At the start of integration, the stress is set to $\tau(t = 0) = 50$ MPa. We solve for the effective temperature on a spatial grid with $nz = 101$ points in the z-direction, which resolves the dynamic evolution of the plastic strain rate within the fault gouge. We solve for the effective temperature in only half of the gouge, as the effective temperature is symmetric about $z = 0$. The spatial derivatives of the effective temperature are split into two terms and are approximated by second order central finite differences, and time integration is performed using a linearly implicit trapezoidal method with an adaptive time step. We use no conduction boundary conditions for the effective temperature at the boundaries of the gouge layer.

The effective temperature dynamically evolves in the STZ model, which leads to a dynamic evolution of the plastic

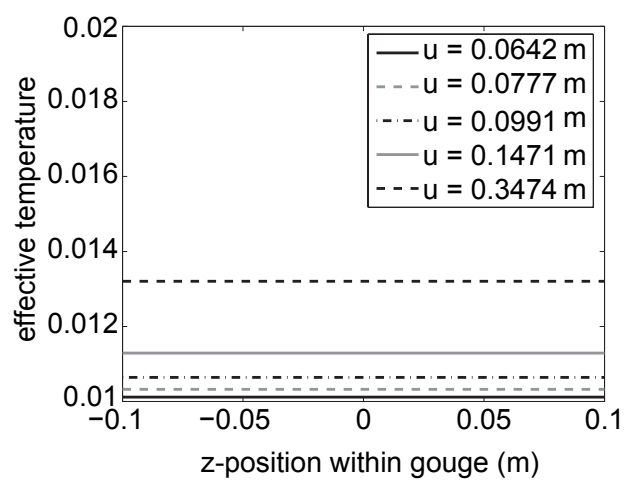

Figure 3. Plot of effective temperature as a function of position at several different values of the shear displacement u for spatially uniform initial conditions. The diffusion term is zero, and by symmetry the effective temperature remains spatially homogeneous as the gouge is sheared.

strain rate in the material. We consider two different types of initial conditions: spatially uniform in the z-direction, and the spatially uniform initial conditions plus a small perturbation. For the spatially uniform case, the initial effective temperature that we use is $\chi(t = 0) = 0.009$. If the initial effective temperature is spatially homogeneous, then by symmetry the strain rate is uniform and the subsequent plastic deformation is spatially uniform in the z-direction (Figure 3). In this case, the PDE for the effective temperature reduces to an ODE because the diffusion term is zero. Frictional behavior for homogeneous initial conditions is similar to that of the Dieterich-Ruina laboratory-based friction laws that are commonly used in earthquake modeling, as was discussed by *Daub and Carlson* [2008].

However, perfectly homogeneous initial conditions are not physically realistic. A spatially uniform initial effective temperature is extremely unlikely, and we approximate real initial conditions by adding a small perturbation (of the form $\delta\chi \cdot \mathrm{sech}(z/\delta w)$, with $\delta\chi = 10^{-10}$ and $\delta w = w/25$). A single perturbation is sufficient to approximate heterogeneous initial conditions because with rate weakening parameters, we find that a single shear band forms at the point with the largest initial effective temperature regardless of the choice of heterogeneous initial conditions. When the initial effective temperature is perturbed, the diffusion term is no longer zero. We use a diffusion constant $D = 0.0001$ m^2 when numerically integrating the STZ equations with the perturbed initial effective temperature.

Figure 4 shows the effective temperature dynamics with a small perturbation added to the initial effective temperature. The perturbation spontaneously grows as the gouge is sheared and a narrow shear band dynamically forms. The unstable growth of the perturbation is due to a feedback in the effective temperature evolution law. Any spatial point with an elevated effective temperature also has a larger strain rate. The energy dissipation term in the effective temperature governing equation (Equation (2)) is proportional to the strain rate, so the effective temperature at a point with an elevated effective temperature grows more rapidly than others. This feeds back into the dissipation term, and leads to strain localization and the formation of a shear band. The final shear band width is determined by the diffusion length scale $\sqrt{D}$, and the steady shear band profile that results balances dissipation and diffusion.

It is important to note that the diffusion of effective temperature occurs in a different manner from thermal diffusion, as the time scale for effective temperature diffusion is set by the inverse plastic strain rate. This means that both the dissipation and diffusion terms are proportional to the plastic strain rate, and can balance each other as long as the strain rate is not above the strain rate at which the effective temperature diverges (q_0/t_0). Because of this difference in time scales between effective temperature diffusion and thermal temperature diffusion, our work provides an alternative

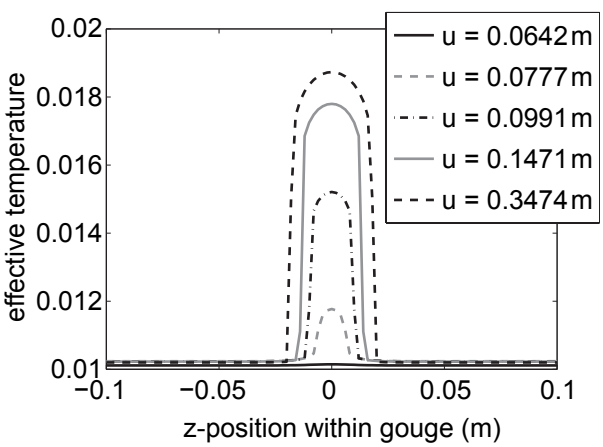

Figure 4. Plot of effective temperature as a function of z-position at several different values of the shear displacement u for the same spatially uniform initial conditions in Figure 3 plus a small perturbation described in the main text. As the gouge is sheared, the perturbation amplifies and grows into a shear band. The effective temperature grows much more rapidly with shear displacement when a shear band forms than when deformation is spatially uniform.

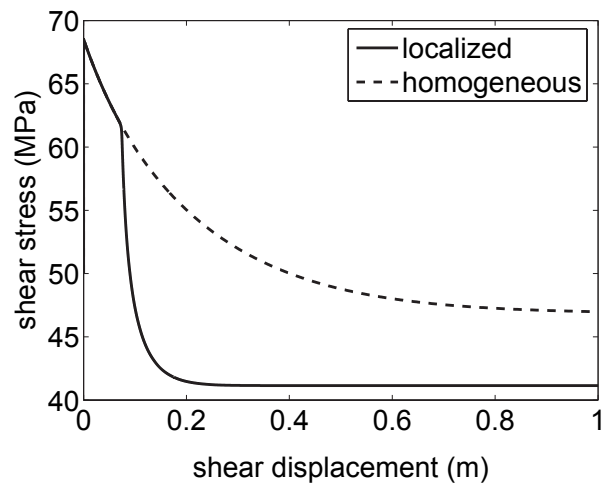

Figure 5. Plots of stress as a function of shear displacement for the plots in Figures 3 and 4. "Homogeneous" indicates that the initial effective temperature is spatially uniform, and the effective temperature for this curve is illustrated in Figure 3. "Localized" indicates that a small perturbation is added to the spatially uniform initial effective temperature; a shear band forms in this case. The effective temperature for the "localized" curve is shown in Figure 4. The formation of a shear band produces different macroscopic material behavior. The shear stress drops more rapidly with shear displacement for "localized" shear, and the steady sliding friction is significantly lower than the "homogeneous" case.

Table 2. Elastodynamic parameters in rupture simulations.

Parameter	Description
$\mu = 32$ GPa	Shear modulus
$c_s = 3.464$ km/s	Shear wave speed
$\nu = 0.25$	Poisson's ratio
$L_{\mathrm{fault}} = 8$ km	Length of fault that can rupture
$L_{\mathrm{trigg}} = 1$ km	Length of triggering patch
$\tau_{\mathrm{trigg}} = 67.5$ MPa	Triggering stress
$dl = 0.005$ km	Grid spacing in the x-direction
$nx = 2048$	Number of grid points in the x-direction
cfl $= 0.3$	Courant-Friedrichs-Lewy Ratio cfl $= c_s dt/dl$
$w = 0.1$ m	Half width of fault gouge layer
$nz = 101$	Number of z-direction grid points spanning half width of gouge
$dz = 0.001$ m	Grid spacing in z-direction
$n_{\mathrm{sub}} = 10$	Substeps within elastodynamic time step for effective temperature integration
$\tau_0 =$ varies	Initial shear stress

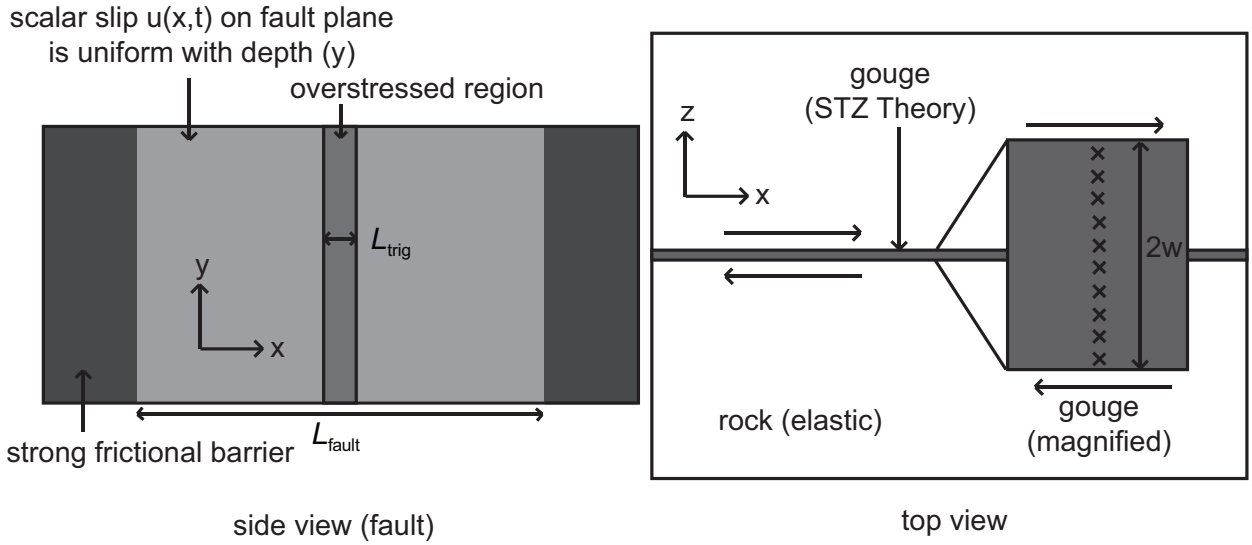

Figure 6. Diagram illustrating the fault in the dynamic rupture model. (left) Side view of the fault plane. Slip is assumed to be uniform with depth. The triggering patch (medium gray) initiates slip, and the rupture spontaneously propagates along strike through the light gray region before it hits the strong barriers (darkest gray) to stop the rupture. (right) Top view of the fault. A thin layer of fault gouge, which is described by STZ Theory, is sheared between elastic rock. Within the fault gouge, we resolve the dynamic evolution of the effective temperature across its width (inset). The effective temperature evolves independently at each position along strike, and dynamic fault slip at each point drives the process of strain localization in the model.

picture to other studies of shear banding that investigate thermal runaway effects [*Kaus and Podladchikov*, 2006].

The prediction that a perturbation to the initial effective temperature results in localization of strain can be confirmed through a linear stability analysis. *Manning, et al.* [2009] found that steady sliding was unstable if $\chi_w < 1$, which is precisely the conditions for steady-state rate weakening. This indicates that if the friction law weakens with strain rate, any perturbation results in localized strain. *Manning, et al.* [2009] also determined that shear bands can form even if the friction law is rate strengthening due to transient effects. While we focus on rate weakening parameters in this study, the prediction that rate strengthening materials can form shear bands has implications for many geophysical systems.

We show a plot of stress as a function of shear displacement for the two different sets of initial conditions in Figure 5. The curve for spatially uniform initial conditions is labeled "homogeneous," and the curve for perturbed initial conditions is labeled "localized." The curves are identical for shear displacements less than 0.1 m, at which point the shear band forms for the perturbed initial conditions. The shear displacement at which localization sets in is determined by the magnitude of the perturbation $\delta\chi$. The larger the value of $\delta\chi$, the more quickly the shear band forms and the less slip required for localization to occur. The width of the perturbation δw has no effect on the friction dynamics – a single shear band of a width determined by the diffusion length scale forms regardless of the choice of δw. Once the shear band forms, the stress drops rapidly and the sliding friction is reduced. This indicates that localization is a mechanism for dynamic weakening. The strain rate is locally higher in the shear band, and the friction law weakens with strain rate, so the shear stress while sliding with a shear band is lower than for the case without a shear band.

The difference in the macroscopic stress shows that strain localization has a significant impact on the frictional properties of fault gouge. In the next section, we examine the implications this has for the larger scale dynamics of earthquake rupture on faults.

4. Dynamic Ruptures With Localization

To investigate the impact of strain localization in dynamic earthquake rupture, we implement the STZ friction law in spontaneous elastodynamic rupture simulations. The elastodynamic response of the surrounding rock is modeled using a boundary integral method [*Cochard and Madariaga*, 1994; *Perrin et al.*, 1995; *Geubelle and Rice*, 1995]. In the boundary integral method, the shear stress τ on the fault can be written

$$\tau(x,t) = \tau_0(x) + \phi(x,t) - \frac{\mu}{2c_s}V(x,t). \qquad (7)$$

The total shear stress on the fault is the combination of three terms: the initial shear stress on the fault $\tau_0(x)$, the stress transfer functional $\phi(x,t)$, and radiation damping. The stress transfer functional accounts for all dynamic stress changes due to prior slip on the fault, and is calculated using FFTs. We note that although the radiation damping term is explicitly written out in Equation (7), the full dynamic response is accounted for with this method. The stress and slip rate also satisfy the friction law (Equation (1)) integrated over the gouge width in the z-direction, and the friction law and elastodynamic equation are solved simultaneously on the fault.

We simulate in-plane dynamic ruptures with the STZ friction law. The fault that we model is illustrated in Figure 6. The left picture shows a side view of the fault plane. We assume that slip does not vary in the y-direction, and that slip occurs only in the x-direction. This geometry allows for both supershear and sub-Rayleigh propagation speeds. For simplicity, we assume that the friction parameters and initial conditions for the effective temperature do not vary along strike (x-direction). Additionally, the initial shear stress is uniform along strike ($\tau_0(x) = \tau_0$) with the exception of a triggering patch of width $L_{\rm trig}$ where the stress is elevated to $\tau_{\rm trig}$ to nucleate rupture. Strong barriers with a large yield stress τ_y stop the rupture once it reaches the edge of the fault. The right picture shows a top view of the fault.

A layer of gouge of half width w, which is described by STZ Theory, is sheared between elastic rock. The inset shows a close up of the fault gouge, where the spatial grid in the z-direction resolves the dynamic evolution of the effective temperature in response to fault slip. Our perturbation to the initial effective temperature is symmetric about $z = 0$, so we only solve for the effective temperature in one half of the gouge layer. The elastodynamic parameters for our simulations are listed in Table 2.

We approximate the spatial derivatives in the effective temperature evolution with central, second order finite differences. Our finite difference scheme separates the diffusion term into two terms, and the differences are computed on a spatial grid in the z-direction spanning the half width of the gouge. The stress is assumed to be constant across the gouge, which means that the spatial variation of the effective temperature determines how strain localizes within the fault core. As with our study of friction dynamics in Section 3, we assume that $\partial\chi/\partial z = 0$ at $z = \pm w$, and assume that the effective temperature is symmetric about $z = 0$.

Our time integration scheme treats the effective temperature derivatives in the diffusion term implicitly, and treats the energy dissipation and relaxation terms explicitly. The energy dissipation term must be treated explicitly in the boundary integral method due to its dependence on the strain rate. The diffusion constant, due to its dependence on the strain rate, must also be treated explicitly. Because of this, the time steps must be small enough to resolve the evolution of the strain rate to determine the correct diffusion time scale. Because the effective temperature (and therefore the strain rate) evolve on a time scale faster than the time for seismic waves to propagate along the fault, our time integration scheme involves taking n_{sub} substeps within an elastodynamic time step to integrate the effective temperature stably, as done in *Noda, Dunham, and Rice* [2009].

As with the smaller scale numerical investigation of friction dynamics, the effective temperature initial conditions determine the subsequent evolution of strain rate in the gouge. If the initial effective temperature is spatially uniform across the width of the gouge (z-direction), we refer to the rupture as "homogeneous." Homogeneous only refers to the strain rate across the width of the gouge at any one spatial point – the effective temperature varies along strike as it evolves in response to slip on the fault, and it is also time dependent. The spatially uniform initial effective temperature in our simulations is identical to the initial effective temperature in the investigation of friction dynamics (Section 3), $\chi(t = 0) = 0.009$.

If the initial effective temperature includes a small perturbation identical to the perturbation in the investigation of friction dynamics (Section 3), then we refer to the rupture as "localized." This means that at any given position, the strain rate can vary across the width of the gouge due to the evolution of the effective temperature. The strain rate profile also varies along strike, as the effective temperature evolves due to rupture propagation. At any given time, there are both spatial points that have not ruptured that still match the initial conditions, as well as points that are actively slipping, where the strain rate profile is determined by the effective temperature evolution.

Additionally, for "localized" ruptures, we examine a variety of different diffusion constants. We choose to vary the diffusion length scale $\sqrt{D}$ because it is not as well constrained as gouge widths that can be observed in the field. Alternatively, the effect of localization can be varied by changing the gouge half width w instead of $\sqrt{D}$, as the ratio $\sqrt{D}/w$ determines the effect of localization on the dynamic rupture.

If the diffusion length scale ($\sqrt{D}$) is smaller than the half width of the gouge w, then a shear band that is narrow on the scale of the gouge forms. This case is refered to as a "narrow shear band." If the diffusion length scale is of the order of the half width of the gouge or larger, then the shear band that forms fills the entire width of the gouge. This case is refered to as a "broad shear band."

The distinction between "broad" and "narrow" shear bands is important because localization is a mechanism for dynamic weakening. The narrower the shear band, the larger the strain rate in the shear band, and the lower the shear stress. We illustrate the effect of changing the diffusion constant in Figure 7. The plot shows the shear stress as a function of slip at a point 2 km from the hypocenter for four different values of the diffusion constant, as well as the same curve for a homogeneous rupture. The plot confirms that narrow shear bands increase the dynamic weakening due to localization, and decrease the sliding friction during earthquake rupture.

A plot of shear stress as a function of slip at a point 2 km from the hypocenter is shown in Figure 8. The shear stress weakens in two distinct phases. For slip less than 0.1 m, stress weakens gradually with slip. This corresponds to an approximately spatially uniform effective temperature, before the shear band grows rapidly. For slip between 0.1 m and 0.3 m, the stress drops rapidly due to the rapid growth of the shear band. Once the stress fully weakens, the stress increases due to re-strengthening. In this case, slip stops shortly before 0.7 m, and the fault heals.

The evolution of the effective temperature during dynamic rupture is similar to its evolution in the simple

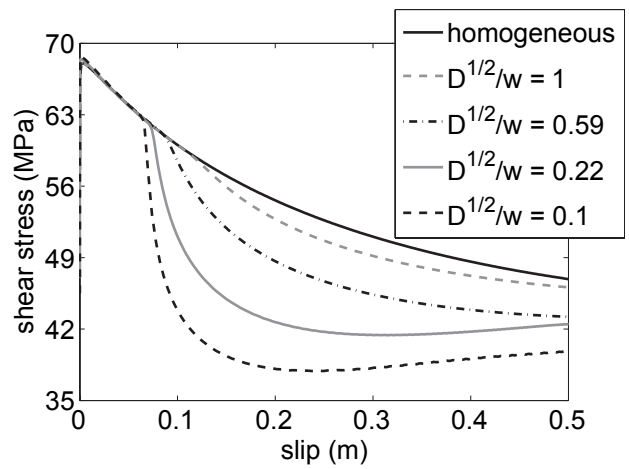

Figure 7. Plot of shear stress as a function of slip for varying diffusion constants scaled by the half-width of the fault gouge $\sqrt{D}/w$ at a point on the fault 2 km from the hypocenter. In each case, the dynamically selected shear band width in the fault gouge is proportional to the effective temperature diffusion length scale. The uppermost curve is a "homogeneous" rupture for comparison, where the initial effective temperature is spatially uniform and no shear band forms. The other curves are all "localized" ruptures. The uppermost curve that includes diffusion ($\sqrt{D}/w = 1$) is a "broad shear band," as the diffusion length scale is equal to the gouge width. The lowermost curve is a "narrow shear band" with a diffusion length scale that is significantly smaller than the gouge half-width ($\sqrt{D}/w = 0.1$). As the diffusion length scale decreases, the shear band becomes narrower, and the stress decreases more rapidly and reaches a lower value. The variation of stress as a function of slip with the diffusion length scale shows that strain localization is a mechanism for dynamic weakening.

sheared layer of gouge. Snapshots of the effective temperature as a function of position within the gouge thickness at several points along the stress versus slip curve are shown in Figure 9. The earliest effective temperature plot shows that during the initial weakening phase of the stress versus slip curve, the gouge deforms approximately homogeneously. This is because the feedbacks in the effective temperature equation require time to amplify heterogeneity in the initial conditions. The duration of this phase of weakening is controlled by the magnitude of the initial perturbation to the effective temperature. Larger initial perturbations require less time to dynamically grow and shorten the amount of slip before the shear band forms.

As the effective temperature in the shear band increases, the shear stress in the gouge drops rapidly with increasing slip. The shear stress is lower because the strain rate is elevated in the shear band, and the STZ friction law weakens with strain rate. Additionally, the stress drops more rapidly because the relevant length scale for friction evolution is now the shear band width ($\sim \sqrt{D}$) instead of the half gouge width w. These two factors combine to significantly reduce the frictional dissipation on the fault during fault slip.

As the successive plots of the effective temperature show, the effective temperature in the shear band grows in magnitude, and the width of the shear band increases as the stress on the fault drops. The expanding width is due to the diffusion of effective temperature. The shear band reaches its maximum width when the stress reaches its minimum value, and the same shear band width is maintained for the duration of slip.

The rapid weakening of the shear stress coincides with the largest strain rates during rupture. Figure 11 shows strain rate profiles across the gouge width at several times during the weakening phase of dynamic rupture. The largest strain rates occur just as the shear band forms. This is because shear stress decreases most rapidly with slip at this time, releasing the most strain energy from the bulk. The strain rate at the center of the gouge decreases as the stress continues to drop with further slip, and the shear band broadens due to diffusion of the effective temperature. Because the slip rate is the strain rate integrated across the width of the gouge, the largest slip rates also occur when the stress decreases most rapidly with slip.

At the scale of faults, ruptures can grow in space and time in a number of ways. Slip can propagate as an expanding crack, where points on the fault continue to slip after the rupture front arrives, or as a self-healing pulse, where at any given point the duration of slip is much shorter than the total time the fault is rupturing. Additionally, because we consider in-plane dynamic ruptures, the crack-like propagation mode can occur at sub-Rayleigh speeds or at supershear speeds. The initial stress is one factor determining the type of rupture growth – supershear rupture tends to occur at high initial stress, sub-Rayleigh rupture at intermediate initial stress, and pulse-like rupture at low initial stress.

The other important factor determining how slip propagates on a fault is the friction law – how much the fault weakens when it slips, and how much energy is dissipated on the fault. Because our simulations show localization decreases the frictional disspation and reduces the shear stress, the width of the shear band in the gouge plays an important role in determining how slip propagates along the fault. We vary the diffusion length scale $\sqrt{D}$, which controls the degree of localization. Small values of the diffusion constant produce narrow shear bands, while larger values of the diffusion constant produce broad shear bands. We vary the diffusion length scale $\sqrt{D}$ over an order of magnitude, ranging

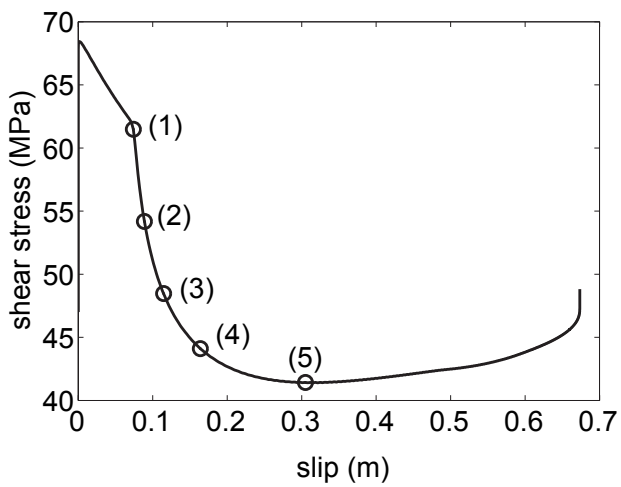

Figure 8. Plot of shear stress as a function of slip at a point on the fault 2 km from the hypocenter. The shear stress drops in two different stages. First is an early stage where the effective temperature is uniform in the fault gouge, which lasts for the first 0.1 m of slip. After about 0.1 m of slip, more rapid dynamic weakening occurs, which is coincident with the shear band formation. Once the stress decreases to its minimum value at 0.3 m of slip, the fault continues to slip and the stress gradually rises. Slightly before 0.7 m of slip is reached, slip ceases and the fault heals, which indicates that slip propagates as a self-healing pusle for these conditions. The diffusion constant in this simulation is $\sqrt{D}/w = 0.2236$, and the initial stress is $\tau_0 = 47$ MPa.

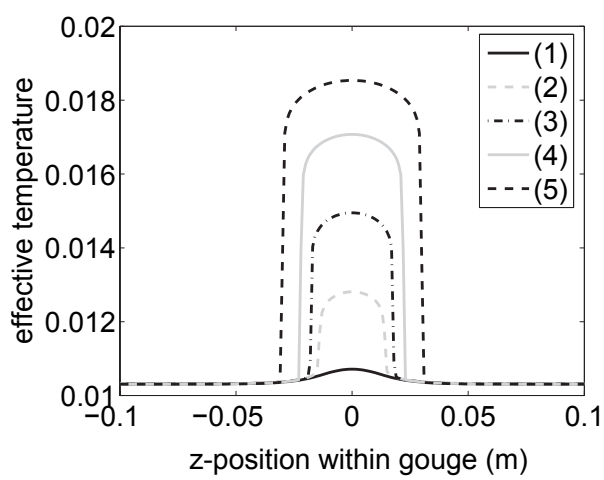

Figure 9. Plot of effective temperature as a function of z-position within the gouge at a point 2 km from the hypocenter at representative points shown in the stress versus slip plot (Figure 8). The horizontal range in this plot shows the entire gouge width in the simulation. The effective temperature is spatially uniform after 0.1 m of slip, at which point the feedbacks amplify the initial perturbation and a shear band forms. As slip propagates, the effective temperature increases and diffuses outwards. For slip beyond 0.3 m, the effective temperature decreases due to the relaxation term and maintains the width in curve (5). The diffusion constant in this simulation is $\sqrt{D}/w = 0.2236$, and the initial stress is $\tau_0 = 47$ MPa.

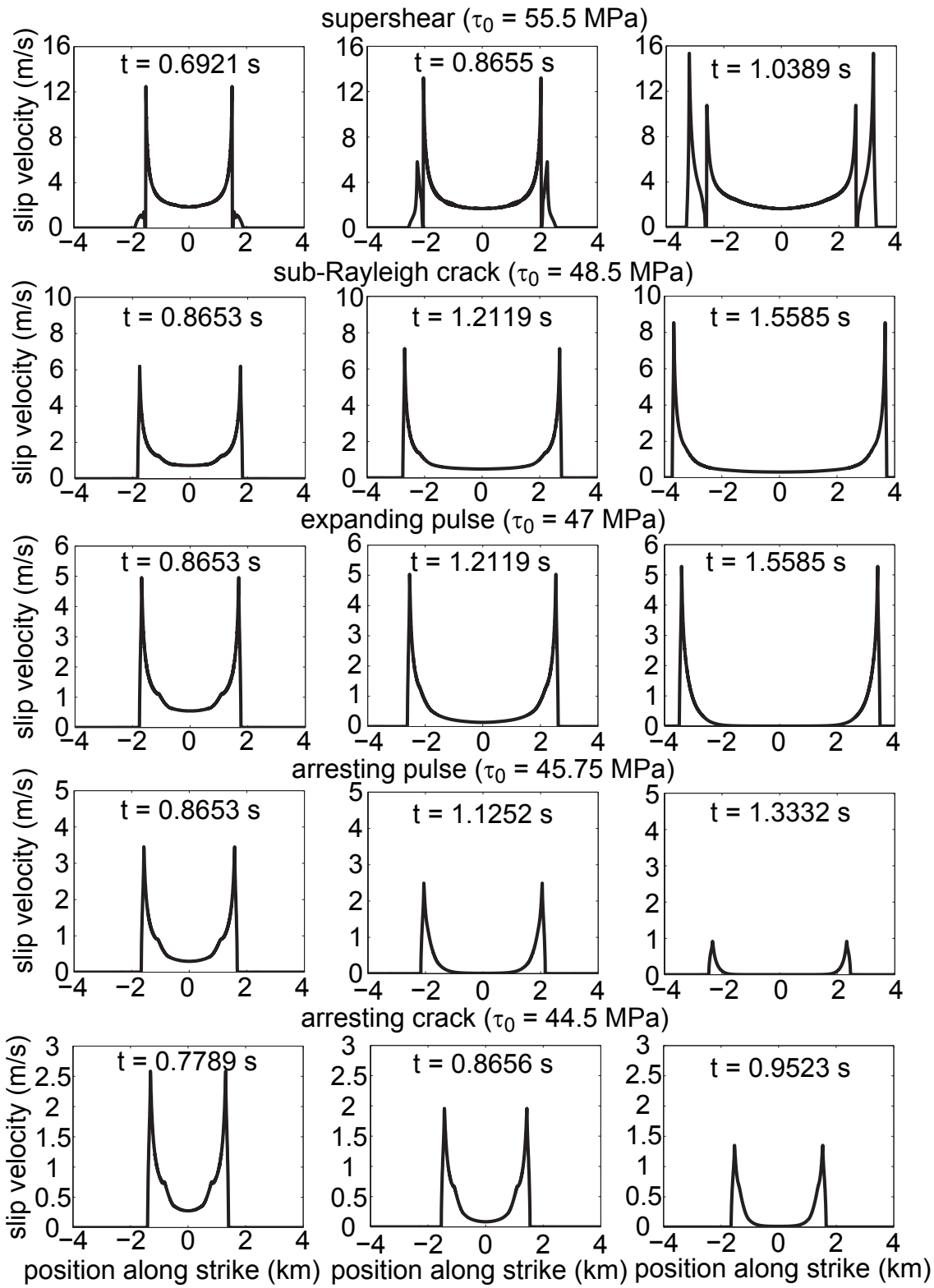

Figure 10. Snapshots of slip rate as a function of position along strike for the various types of rupture. The effective temperature diffusion constant in these simulation is $\sqrt{D}/w = 0.2236$. At the largest stress ($\tau_0 = 55.5$ MPa), slip nucleates ahead of the rupture rupture front and propagates faster than the shear wave speed. Crack-like rupture traveling sub-Rayleigh speeds occurs at an intermediate stress ($\tau_0 = 48.5$ MPa). The rupture propagates as a self-healing pulse for lower shear stress, and can rupture the entire fault as a pulse ($\tau_0 = 47$ MPa), or slip can arrest before the pulse reaches the edge of the fault ($\tau_0 = 45.75$ MPa). For the lowest values of shear stress ($\tau_0 = 44.5$ MPa), slip arrests while the rupture is still a crack. While the arresting ruptures look very similar, they are classified differently because the arresting pulse meets our criterion for pulse-like rupture described in the main text, while the arresting crack does not.

cannot drop below the yield stress to cause fault slip to completely cease. We therefore define a pulse-like rupture when the slip rate at the center of the fault is three orders of magnitude smaller than the peak slip rate at the rupture front.

We illustrate the different ways that slip propagates on the fault for a value of the diffusion constant that allows for pulse-like rupture ($D = 0.0005$ m^2, $\sqrt{D}/w = 0.2236$) in Figure 10. Pulse-like rupture does not occur for all values of the diffusion constant, only for smaller values that provide more dynamic weakening. If the initial stress is $\tau_0 = 55.5$ MPa, then the rupture propagates as a supershear crack. Slip initiates ahead of the sub-Rayleigh crack tip and grows unstably, as the series of plots of slip rate as a function of position along strike illustrate.

If the initial stress is $\tau_0 = 48.5$ MPa, fault slip occurs as an expanding sub-Rayleigh crack. In this series of snapshots of slip rate as a function of position, once slip initiates at a given point, the point continues to slip until the rupture reaches the boundary of the fault. This type of rupture occurs for intermediate values of the shear stress.

For lower values of the shear stress, rupture propagates as an expanding, self-healing pulse. This type of rupture is illustrated for $\tau_0 = 47$ MPa. The rupture begins as an expanding crack as shown in the top plot of slip rate as a function of position along strike, but then slip stops in the center of the fault and the subsequent propagation is pulse-like. In this type of rupture, a given point slips for less time than the duration of the entire earthquake.

If the initial stress is too low, the dynamic rupture cannot propagate over the entire spatial extent of the fault. Arresting ruptures can be pulse-like, where the rupture transitions to pulse-like rupture but arrests before it reaches the fault boundary, or crack-like, where the rupture arrests while it is an expanding crack. An example of an arresting pulse and an example of an arresting crack are shown in Figure 10.

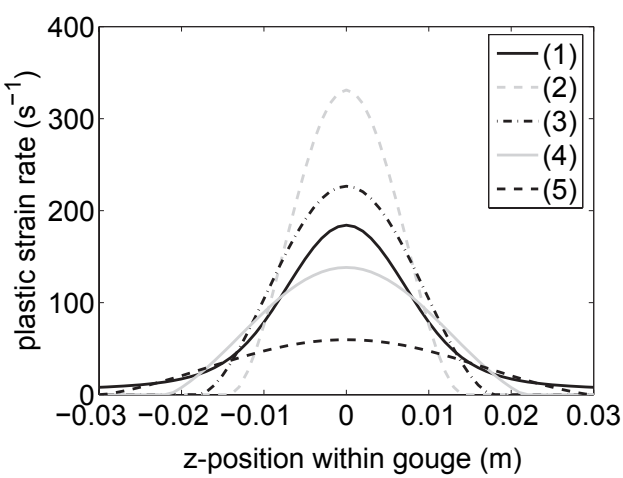

Figure 11. Plot of plastic strain rate as a function of position within the gouge at a point 2 km from the hypocenter at representative points shown in the stress versus slip plot (Figure 8). Note that the horizontal range in this plot is smaller than in Figure 9, as the strain rate is more sharply peaked than the effective temperature. The largest strain rate occurs early in the weakening process, as this is when the stress drops most rapidly with slip and releases elastic strain energy from the bulk at the largest rate. The diffusion constant in this simulation is $\sqrt{D}/w = 0.2236$, and the initial stress is $\tau_0 = 47$ MPa.

While the slip rate as a function of position look similar for the two ruptures, the arresting pulse meets our criteria for pulse-like rupture while the arresting crack does not. The arresting pulse occurs for $\tau_0 = 45.75$ MPa, and for even lower stresses the rupture arrests before the rupture becomes pulse-like ($\tau_0 = 44.5$ MPa).

We determine the range of stresses that produce each different type of rupture for multiple values of the diffusion length scale. This produces a diagram that indicates rupture type as a function of the diffusion length scale and the initial stress (Figure 12). For each value of the initial stress and each value of the diffusion constant, a corresponding point can be located on the plot. Points corresponding to example plots showing the different rupture types (Figure 10) are indicated on the plot as circles. For a specific choice of parameters (D and τ_0), the region where this point falls determines the type of rupture that our simulation produces.

As expected, the additional weakening and reduced frictional dissipation for the more localized ruptures reduces the minimum shear stress for all types of rupture. The upper curve (gray) in Figure 12 is the minimum stress needed to nucleate supershear rupture. An order of magnitude reduction in the diffusion constant reduces the minimum stress needed to nucleate supershear rupture by about 7 MPa. This is a significant fraction of the initial shear stress on the fault, and shows that the reduction in frictional energy

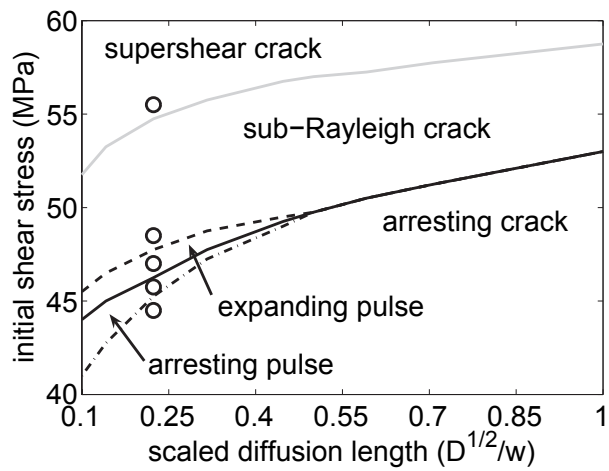

Figure 12. Rupture classification diagram as a function of diffusion length scale and initial shear stress for ruptures with STZ Theory. For a given value of the initial shear stress and the diffusion length scale, the region that the point falls into determines the type of rupture that is observed. For larger values of the diffusion length scale (i.e. "broad shear bands"), slip can propagate as a supershear crack, sub-Rayleigh crack, or arresting crack only. For smaller values of the diffusion length scale (i.e. "narrow shear bands"), slip can also propagate as an expanding or arresting pulse. The pulse-like rupture can occur for narrow shear bands because of the dynamic weakening provided by strain localization. The rupture with the narrowest shear band that we simulated reduces the minimum stress required for slip to propagate on the fault (solid black line) relative to the broadest shear band by 9 MPa, which is a significant fraction of the initial stress on the fault. The circles on the diagram indicate the specific examples of ruptures that are shown in Figure 10.

dissipation and the increase in dynamic weakening due to localization can signficantly alter how slip propagates on the fault.

The lower curves (black) in Figure 12 indicate how localization affects rupture propagation at lower initial shear stress. For broad shear bands, slip can only grow in a crack-like manner, but as the diffusion constant is decreased, pulse-like rupture can occur. This is because localization leads to additional dynamic weakening, which was shown to be the crucial frictional characteristic determining when slip propagates as a self-healing pulse by *Zheng and Rice* [1998]. The solid line marks the lowest stress required to propagate slip over the entire fault. This involves crack-like rupture if $\sqrt{D} > 0.5w$ and pulse-like rupture if $\sqrt{D} < 0.5w$. The initial stress needed to fully rupture the fault (solid black) decreases by nearly 10 MPa over the range of diffusion constants that we simulated. This is also a significant fraction of the initial shear stress. As with the supershear rupture transition, the small scale process of localization can alter the manner in which slip propagates at the fault scale.

5. Discussion

Our simulations with the STZ friction law reveal that the dynamic weakening provided by localization can have a significant impact on fault dynamics. In the STZ model, shear bands spontaneously form and grow in response to dynamic fault slip. This provides a unique description of fault friction. Rather than assuming planar slip with a slip-weakening or Dieterich-Ruina friction law, the dynamic evolution of the effective temperature determines the strain rate in the fault zone.

Strain localization alters the stress drop and slip rate of dynamic rupture. The stress drop in a simulation that dynamically forms a shear band is larger than if no shear band forms. The peak slip rate is also larger in simulations that form shear bands because the stress weakens over a smaller slip length scale and releases stored elastic energy more rapidly. Ground motion away from the fault tends to be larger if the peak slip rate is increased [*Aagard et al.*, 2001], which suggests that strain localization may impact the ground motion in real earthquakes.

Additionally, we find that localization plays an important role in determining rupture propagation speeds. The stress which marks the transition to supershear changes by a significant amount for the narrowest shear bands. There is evidence of supershear rupture speeds in many earthquakes [*Archuleta*, 1984; *Bouchon et al.*, 2001; *Bouchon and Vallée*, 2003; *Ellsworth et al.*, 2004], as well as observations of supershear rupture in laboratory slip experiments [*Rosakis et al.*, 1999]. Supershear ruptures radiate seismic waves with a distinct attenuation pattern compared to sub-Rayleigh ruptures [*Dunham and Archuleta*, 2005]. Therefore, understanding the conditions which lead to supershear rupture is important for determining seismic ground motions.

In our simulations, localization provides the dynamic weakening necessary for pulse-like rupture. Our simulations do not produce pulse-like ruptures for homogeneous deformation because there is not enough frictional weakening to allow for pulses in the absence of strain localization. Strain localization reduces the minimum initial stress for the earthquake to rupture the entire fault by about 10 MPa, a significant amount relative to the initial stress on the fault. Seismic observations suggest pulse-like rupture propagation in many earthquakes [*Heaton*, 1990]. *Zheng and Rice* [1998] determined that pulse-like rupture tends to occur for low initial shear stress and with friction laws that exhibit increased velocity weakening in steady state. Our simulations are consistent with their results, as pulses occur at lower initial shear stresses for the narrower shear bands, where there is more dynamic weakening.

In our study, we vary the effective temperature diffusion length scale over an order of magnitude to determine how the amount of dynamic weakening impacts the propagation of ruptures. This parameter is selected because the diffusion length scale is poorly constrained, and because it is difficult to predict precisely what the shear band width will be for a given set of parameters. The final shear band width that the material chooses is dynamically selected by a balance between the nonlinear processes of energy dissipation, effective temperature diffusion, and healing. The width is proportional to the diffusion length scale $\sqrt{D}$, but it also depends on the stress, the effective temperature, and the effective temperature specific heat.

We consider a range of effective temperature diffusion length scales because simulations, experiments, and field observations yield a wide range of shear band thicknesses in amorphous materials. Simulations of glassy materials indicate that shear band thicknesses tend to be approximately 10 particle diameters [*Falk and Langer*, 1998], though for granular materials this could be very different because particles have a greater variety of sizes. *Morgan and Boettcher* [1999] determined that deformation in numerical simulations of fault gouge tends to localize to a narrower shear band when a particle size distribution more heavily weighted towards small particles is used. In each of their simulations, the shear band is only a few particle diameters wide. However, simulations do not include the full range of particle sizes that are found in natural faults [*Chester et al.*, 2005]. Experimental investigations of shear band thicknesses in granular materials indicate that shear band thickness should scale with the "mean particle diameter," defined such that 50% of the particles by weight have larger size [*Tordesillas et al.*, 2004]. Rock mechanics studies on laboratory faults with gouge observe shear band thicknesses that depend on the grain sizes, with the shear band thicknesses ranging from around 100 μm [*Beeler et al.*, 1996] to several millimeters [*Chambon et al.*, 2006]. The thickness of shear bands in natural faults range from hundreds of microns to a few millimeters [*Chester et al.*, 1993; *Chester and Chester*, 1998; *Wibberley and Shimamoto*, 2003].

The thicknesses of slip zones observed in exhumed faults are even narrower than the shear bands in our simulations [*Chester et al.*, 1993; *Chester and Chester*, 1998; *Wibberley and Shimamoto*, 2003], indicating that the dynamic weakening from strain localization could be even more dramatic than our results indicate. We did not explore smaller diffusion length scales due to computational limits – the effective temperature grid must be fine enough to resolve the shear band, and the narrower shear bands reduce the slip scale over which the stress weakens. This rapid stress drop requires a smaller grid spacing along strike to produce well resolved simulations.

Laboratory experiments on simulated fault gouge indicate that strain localization, dilation, and frictional rate dependence are interrelated [*Beeler et al.*, 1996; *Mair and Marone*, 1999]. Fault gouge tends to produce rate strengthening behavior when significant layer dilation occurs for small strains, and rate weakening behavior at larger strains once strain localizes. Effective temperature is a generalization of free volume [*Langer*, 2008], and so we expect regions of high effective temperature to have a higher free volume and porosity. Because of this, STZ Theory predicts that a homogeneously deforming layer dilates more than a layer with a localized shear band, which is what is observed experimentally. The effective temperature for homogeneous deformation is spatially uniform, while the effective temperature for deformation with a shear band is locally higher in the narrow shear band, and lower everywhere else. The average effective temperature is larger for the spatially uniform effective temperature, and therefore the free volume

and porosity are larger, but the average strain rate is the same due to the nonlinear relationship between effective temperature and the plastic strain rate (Equation (1)). The experiments also indicate a transition from rate strengthening to rate weakening as localization occurs. In the STZ model as presented in this study, the rate dependence of friction is independent of the degree of localization. However, the transition from rate strengthening for homogeneous deformation to rate weakening for localized deformation can be incorporated by modifying the strain rate dependence of the maximum effective temperature (Equation (3)) to the form used in *Manning et al.* [2009].

Another important question that arises in the context of laboratory experiments is if the dynamic weakening predicted by STZ Theory could be observed in an experiment. This is a difficult problem, as the experiment must be able to distinguish between homogeneous and localized deformation over the course of a single friction experiment. Studies such as the *Beeler et al.* experiments do not observe friction versus displacement curves like those in our study, even though deformation localizes to a narrow shear band. However, the absence of such weakening could be due to deformation localizing to a shear band from the beginning of the experiment, as the two stage weakening we observe requires a brief period of homogeneous deformation. Experiments that can actively image particle displacements during shear, such as those that use photoelastic beads [*Daniels and Hayman*, 2008], might be better suited to determining if localization produces the dynamic weakening predicted by STZ Theory.

Core samples from the creeping section of the San Andreas Fault Observatory at Depth (SAFOD) indicate that slip occurs throughout the entire gouge width of about 2-3 m (i.e. not localized within the layer) [*Hickman et al.*, 2007]. Laboratory experiments with gouge from the creeping section indicate rate strengthening friction parameters [*Carpenter et al.*, 2007]. These results are consistent with STZ Theory, which predicts that rate strengthening materials form shear bands only as transient phenomena [*Manning et al.*, 2009]. When a rate strengthening material is loaded at a relatively constant rate, STZ Theory predicts that steady sliding is stable and deformation is accomodated over the entire width of the fault gouge, in agreement with the SAFOD experiment.

Slip surfaces are often observed at the boundary between gouge and the host rock in both exhumed faults [*Chester and Chester*, 1998] and laboratory experiments [*Beeler et al.*, 1996]. In STZ Theory, the position where the shear band forms depends on where the initial effective temperature is largest. If there are two or more positions with an equally large initial effective temperature, strain localizes to one. If one of the possible locations is at the boundary, the shear band prefers to form at the boundary rather than in the interior of the gouge layer. Boundary conditions on the effective temperature may also play a role. Our simulations use no conduction boundary conditions, but other boundary conditions, such as fixed effective temperature at the boundary could also be chosen. These may yield different results for the preferred shear band location. Changing the boundary conditions is not likely to be important for shear bands that form in the center of the gouge, but could have an effect on shear bands that form near the gouge/rock boundaries.

Localization of deformation can occur in other models of plasticity [*Rudnicki and Rice*, 1975]. The STZ model has some important differences from the plasticity models in *Rudnicki and Rice*, the most important of which is the inclusion of a length scale that sets the width of shear bands. Dynamic rupture calculations with a *Rudnicki and Rice*-type plasticity model resulted in localization of deformation down to the numerical grid scale even as the grid scale was refined [*Templeton and Rice*, 2008]. In these models, a localization-limiting procedure is necessary for a continuum solution to exist [*Bazant and Jirasek*, 2002]. In STZ Theory, the inclusion of the diffusion length scale limits localization to a minimum shear band thickness, and allows a dynamic balance between dissipation and diffusion to set the shear band thickness. The *Rudnicki and Rice* study found that conditions for localization are normal-stress dependent. This differs from STZ Theory, where the conditions for localization are dependent only on the internal structure of the material through the dynamics of the effective temperature. The normal stress sets the overall stress scael in the problem and plays a role in determining if plastic yielding occurs, as the yield stress could be normal stress dependent, but localization is entirely due to the dynamic instability in the evolution of the effective temperature.

STZ Theory provides a microscopic physical basis for plastic deformation in fault gouge. There are also many other processes that are important during seismic slip which are likely to couple to the STZ dynamics, and are not yet incorporated into STZ Theory. Brittle fracture, wear, and comminution create the finely grained gouge in the fault zone. Fracturing rock dissipates energy and creates smaller grains, which might change parameters such as the effective temperature diffusion length scale or the STZ reversal time scale. Thermal heating and weakening, melting, and pressurization of fluids are also believed to be important during fault slip [*Lachenbruch*, 1980; *Tullis and Goldsby*, 2003; *Di Toro et al.*, 2004; *Di Toro et al.*, 2006; *Rice*, 2006]. These processes likely influence the rate at which STZs reverse and how the effective temperature evolves. Determining how these additional processes couple to the STZ friction law may provide further constraints on the physics of the earthquake source.

Appendix A: Full Derivation of the STZ Equatioins

STZ Theory calculates the plastic strain rate $\dot{\gamma}$ based on four quantities: the shear stress τ, the number of STZs in each of the two possible orientations n_+ and n_-, and the effective temperature χ [*Langer*, 2008]. The number of STZs in each orientation and the effective temperature quantify the internal state of the material. In this paper we incorporate a typical approximation which assumes the number of STZs in each orientation is equal to its steady state value. This approximation is valid when the STZ time scale is much faster than other dynamical processes in the problem. Here, we present the details of the derivation of the STZ equations and the simplifying assumptions necessary for setting the STZ populations to steady state.

In STZ Theory, plastic strain occurs in localized regions that are susceptible to rearrangement under applied shear stress. These regions, called Shear Transformation Zones (STZs), switch between two metastable orientations, denoted "positive" and "negative." When a "positive" orientation changes to a "negative" orientation, the plastic strain increases by a fixed increment, and when a "negative" orientation switches to a "positive" orientation, the plastic strain decreases by a fixed increment. An STZ undergoing a switch from "positive" to "negative" is shown at the right in Figure 1. Once an STZ has switched to the "negative" orientation, the material cannot shear further at that location. Therefore, to accumulate shear the material is constantly creating and destroying STZs as energy is dissipated in the system.

Quantitiatively, the basic premise of STZ Theory can be written as follows:

$$\dot{\gamma} = \frac{2\epsilon}{n_\infty t_0} \left[R\left(+\tau\right) n_+ - R\left(-\tau\right) n_- \right]. \tag{A1}$$

The plastic strain rate $\dot{\gamma}$ is the net sum of all the STZ reversals in the material. The function $R(\tau)$ describes the rate at which STZ reversals take place in response to the applied shear stress. The other parameters are the strain increment per STZ reversal ϵ, a reference STZ population n_∞, and the time scale for STZ reversals t_0.

Equation (A1) can be rewritten with the following change of variables:

$$\Lambda = \frac{n_+ + n_-}{n_\infty},\ m = \frac{n_- - n_+}{n_+ + n_-}. \tag{A2}$$

The variable Λ is proportional to the total number of STZs, and m quantifies the bias. With these variables, the constitutive law becomes

$$\dot{\gamma} = \frac{2\epsilon}{t_0}\mathcal{C}(\tau)\Lambda\left[\mathcal{T}(\tau) - m\right]. \tag{A3}$$

The rate switching funtion is rewritten in the combinations $\mathcal{C}(\tau) = (R(\tau) + R(-\tau))/2$ and $\mathcal{T}(\tau) = (R(\tau) - R(-\tau))/(R(\tau) + R(-\tau))$ in this version of the constitutive law.

In this study, we assume an exponential form for the rate switching function [*Eyring*, 1936]:

$$R(\tau) = \exp\left(-E_0 + \tau/\sigma_d\right). \tag{A4}$$

The rate switching function depends on an activation stress σ_d, and an activation energy scaled by the energy required to form an STZ E_0. The activation stress is known as the direct effect stress in rock mechanics experiments – its magnitude is typically much less than the shear stress ($\tau/\sigma_d >> 1$). This form for $R(\tau)$ reproduces the logarithmic rate dependence seen in rock mechanics experiments [*Daub and Carlson*, 2008]. The rate switching function combinations are then $\mathcal{C}(\tau) = \exp(-E_0)\cosh(\tau/\sigma_d)$ and $\mathcal{T}(\tau) = \tanh(\tau/\sigma_d)$. Under the approximation that $\tau/\sigma_d >> 1$, we set $\mathcal{T}(\tau) \approx 1$.

The STZ populations dynamically evolve as the material is sheared. The STZs can switch between the two orientations, and STZs are created and destroyed. Therefore, the evolution equations for the STZ populations are

$$\begin{aligned}\frac{dn_\pm}{dt} &= \frac{1}{t_0}\left[R(\mp\tau)\,n_\mp - R(\pm\tau)\,n_\pm\right] \\ &\quad + \frac{\dot{\gamma}\tau}{\epsilon\left(n_+ + n_-\right)\tau_y}\left[\frac{n_\infty}{2}\exp\left(-1/\chi\right) - n_\pm\right].\end{aligned} \tag{A5}$$

The first term accounts for STZs switching from "positive" to "negative" and vice versa, and the second term incorporates STZ creation and annihilation. The overall creation/annihilation rate is proportional to the rate at which work is done on the material. The creation term includes effective temperature dependence, as we assume that energy dissipation in the material drives the STZ population towards a Boltzmann distribution. The stress τ_y determines the fraction of dissipated energy that creates STZs, and it also turns out to be the threshold stress that must be applied to switch an STZ.

In the Λ and m variables, the evolution equations become

$$\frac{d\Lambda}{dt} = \frac{\dot{\gamma}\tau}{n_\infty\Lambda\tau_y}\left[\exp\left(-1/\chi\right) - \Lambda\right]; \tag{A6}$$

$$\frac{dm}{dt} = \frac{\dot{\gamma}}{\epsilon n_\infty\Lambda}\left\{1 - \frac{\tau m}{\tau_y}\left[1 + \exp\left(-1/\chi\right) - \Lambda\right]\right\}. \tag{A7}$$

We note that the dynamic equations for Λ and m both have a factor of $1/(n_\infty\Lambda)$. For the equations of STZ Theory to be valid, STZs must be rare, otherwise the assumption that plastic strain occurs in local, isolated regions is no longer valid. Therefore, the number of STZs is small, and the STZ populations evolve quickly relative to the stress and effective temperature. The total number of STZs is always at its steady state value $\Lambda = \exp(-1/\chi)$, which is set by the effective temperature.

If we set the total number of STZs to steady state, then the steady state value for the STZ bias is $m = \tau_y/\tau$. However, the STZ bias cannot be larger than $m = 1$, which corresponds to all the STZs in the "negative" orientation. When all the STZs are in the "negative" orientation, the material cannot be sheared further because there are no regions susceptible to deformation. This means that if $\tau < \tau_y$, then the material is jammed and $\dot{\gamma} = 0$. Otherwise, the material flows. Therefore, the steady state value for the STZ bias is dependent on the stress as follows:

$$m = \begin{cases} 1, & \tau < \tau_y; \\ \tau_y/\tau, & \tau \geq \tau_y. \end{cases} \tag{A8}$$

The STZ dynamics are important for determining if the material is jammed or flowing, but otherwise the stress and effective temperature have a greater effect on the friction dynamics.

The friction law that we use in our simulations is therefore

$$\dot{\gamma} = \frac{2\epsilon}{t_0}\exp\left(-E_0\right)\cosh\left[\tau/\sigma_d\right]\exp\left(-1/\chi\right)\left[1 - \frac{\tau_y}{\tau}\right], \tag{A9}$$

except if $\tau < \tau_y$, when $\dot{\gamma} = 0$. This is the exact version of Equation (1) in the main text. The strain rate depends on the shear stress, and the internal state of the material is described entirely by the effective temperature. We discuss the dynamic equation for the effective temperature in Section 2 in the main text.

Acknowledgments. The authors thank Eric Dunham for providing the dynamic rupture code used in this study and two anonymous reviewers for their comments. This work was supported by the David and Lucile Packard Foundation, NSF grant number DMR-0606092, and the NSF/USGS Southern California Earthquake Center, funded by NSF Cooperative Agreement EAR-0106924 and USGS Cooperative Agreement 02HQAG0008. The SCEC contribution number for this paper is 1303.

References

Aagard, B. T., J. F. Hall, and T. H. Heaton (2001), Characterization of near-source ground motions with earthquake simulations, *Earthquake Spectra*, *17*, 177-207.

Andrews, D. J. (1976a), Rupture propagation with finite stress in antiplane strain, *J. Geophys. Res.*, *81*, 3575-3582.

Andrews, D. J. (1976b), Rupture velocity of plane strain shear cracks, *J. Geophys. Res.*, *81*, 5679-5687.

Archuleta, R. J. (1984), A faulting model for the 1979 Imperial Valley earthquake, *J. Geophys. Res.*, *89*, 4559-4585.

Beeler, N. M., T. E. Tullis, M. L. Blanpied, and J. D. Weeks (1996), Frictional behavior of large displacement faults, *J. Geophys. Res.*, *101*(B4), 8697-8715.

Bizzarri, A., and M. Cocco (2005), 3D dynamic simulations of spontaneous rupture propagation governed by different constitutive laws with rake rotation allowed, *Ann. Geophys.*, *48*(2), 279-299.

Bouchon, M., M. P. Bouin, H. Karabulut, M. N. Toksöz, M. Dietrich, and A. Rosakis (2001), How fast is rupture during an earthquake? New insights from the 1999 Turkey earthquakes, *Geophys. Res. Lett.*, *28*(14), 2723-2726, doi:10.1029/2001GL013112.

Bouchon, M., and M. Vallée, (2003), Observation of long supershear rupture during the magnitude 8.1 Kunlunshan Earthquake, *Science*, *301*, 824-826, doi:10.1126/science.1086832.

Carlson, J. M, and J. S. Langer (1989), Mechanical model of an earthquake fault, *Phys. Rev. A*, *40*, 6470-6484.

Carpenter, B. M., C. J. Marone, and D. M. Saffer (2007), Frictional behavior of materials in the 3D SAFOD volume, *Eos Trans. AGU*, *88*(52), Fall Meet. Suppl., Abstract T41B-0580.

Chambon, G., J. Schmittbuhl, and A. Corfdir (2006), Frictional response of a thick gouge sample: 1. Mechanical measurements and microstructures, *J. Geophys. Res.*, *111*, B09308, doi:10.1029/2003JB002731.

Chester, F. M., and J. S. Chester (1998), Ultracataclasite structure and friction processes of the Punchbowl fault, San Andreas system, California, *Tectonophysics*, *295*, 199-221.

Chester, J. S., F. M. Chester, and A. K. Kronenberg (2005), Fracture surface energy of the Punchbowl fault, San Andreas system, *Nature*, *437*, 133-136, doi:10.1038/nature03942.

Chester, F. M., J. P. Evans, and R. L. Biegel (1993), Interal structure and weakening mechanisms of the San Andreas Fault, *J. Geophys. Res.*, *98*(B1), 771-786.

Cochard, A., and R. Madariaga (1994), Dynamic faulting under rate-dependent friction, *Pure Appl. Geophys.*, *142*(3-4), 419-445.

Cochard, A., and R. Madariaga (1996), Complexity of seismicity due to highly rate-dependent friction, *J. Geophys. Res.*, *101*, 25321-25336, doi:10.1029/96JB02095.

Daniels, K. E., and N. W. Hayman (2008), Force chains in seimogenic faults visualized with photoelastic granular shear experiments, *J. Geophys. Res.*, *113*, B11411, doi:10.1029/2008JB005781.

Daub, E. G., and J. M. Carlson (2008), A constitituve model for fault gouge deformation in dynamic rupture simulations, *J. Geophys. Res.*, *113*, B12309, doi:10.1029/2007JB005377.

Daub, E. G., M. L. Manning, J. M. Carlson (2008), Shear strain localization in elastodynamic rupture simulations, *Geophys. Res. Lett.*, *35*, L12310, doi:10.1029/2008GL033835.

Dieterich, J. H. (1972), Time-dependent friction in rocks, *J. Geophys. Res.*, *77*(20), 3690-3697.

Dieterich, J. H. (1979), Modeling of rock friction 1. Experimental results and constitutive equations, *J. Geophys. Res.*, *84*(NB5), 2161-2168.

Di Toro, G., D. L. Goldsby, and T. E. Tullis (2004), Friction falls towards zero in quartz rock as slip velocity approaches seismic rates, *Nature*, *427*, 436-439.

Di Toro, G., T. Hirose, S. Nielsen, G. Pennacchioni, and T. Shimamoto (2006), Natural and experimental evidence of melt lubrication of faults during earthquakes, *Science*, *311*, 647-649.

Dunham, E. M., and R. J. Archuleta (2005), Near-source ground motion from steady state dynamic rupture pulses, *Geophys. Res. Lett.*, *32*, L03302, doi:10.1029/2004GL021793.

Ellsworth, W. L., M. Celebi, J. R. Evans, E. G. Jensen, R. Kayen, M. C. Metz, J. D. Nyman, J. W. Roddick, P. Spudich, and C. D. Stevens, (2004), Near-field ground motion of the 2002 Denali Fault, Alaska, earthquake recorded at pump station 10, *Earthquake Spectra*, *20*(3), 597-615.

Eyring, H. J. (1936), Viscosity, plasticity, and diffusion as examples of absolute reaction rates, *J. Chem. Phys.*, *4*, 283.

Falk, M. L., and J. S. Langer (1998), Dynamics of viscoplastic deformation in amorphous solids, *Phys. Rev. E*, *57*(6), 7192-7205.

Falk, M. L., and J. S. Langer (2000), From simulation to theory in the physics of deformation and fracture, *MRS Bull.*, *25*(5), 40-45.

Geubelle, P. H., and J. R. Rice (1995), A spectral method for 3-dimensional elastodynamic fracture problems, *J. Mech. Phys. Solids*, *43*(11), 1791-1824.

Haxton, T. K., and A. J. Liu (2007), Activated dynamics and effective temperature in a steady state sheared glass, *Phys. Rev. Lett.*, *99*, 195701.

Heaton, T. H. (1990), Evidence for and implications of self-healing pulses of slip in earthquake rupture, *Phys. Earth Planet. Inter.*, *64*(1), 1-20.

Hickman, S. H., M. D. Zoback, W. L. Ellsworth, D. Kirschner, and J. Solum (2007), Structure and composition of the San Andreas Fault at seismogenic depths: recent results from the SAFOD experiment, *Eos Trans. AGU*, *88*(52), Fall Meet. Suppl., Abstract T44B-01.

Ida, Y. (1972), Cohesive force across the tip of a longitudinal-shear crack and Griffith's specific surface energy, *J. Geophys. Res.*, *77*(20), 3796-3805.

Kaus, P. J. P., and Y. Y. Podladchikov (2006), Initiation of localized shear zones in viscoelastoplastic rocks, *J. Geophys. Res.*. *111*, B04412, doi:10.1029/2005JB003652.

Lachenbruch, A. H., (1980), Frictional heating, fluid pressure, and the resistance to fault motion, *J. Geophys. Res.*, *85*(NB11), 6097-6112.

Langer, J. S. (2008), Shear-transformation-zone theory of plastic deformation near the glass transition, *Phys. Rev. E*, *77*, 021502.

Langer, J. S., and M. L. Manning (2008), Steady-state, effective-temperature dynamics in a glassy material, *Phys. Rev. E*, *76*, 056107.

Lemaitre, A., and J. M. Carlson (2004), Boundary lubrication with a glassy interface, *Phys. Rev. E*, *69*(6), 061611.

Lois, G., A. Lemaitre, and J. M. Carlson (2005), Numerical tests of constitutive laws for dense granular flows, *Phys. Rev. E*, *72*, 051303.

Mair, K., and C. J. Marone (1999), Friction of simulated fault gouge for a wide range of velocities and normal stresses, *J. Geophys. Res.*, *104*(B12), 18,899-28,914, doi:10.1029/1999JB900279.

Manning, M. L., E. G. Daub, J. S. Langer, and J. M. Carlson (2009), Rate-dependent shear bands in a shear-transformation-zone model of amorphous solids, *Phys. Rev. E*, *79*, 016110.

Manning, M. L., J. S. Langer, and J. M. Carlson (2007), Strain localization in a shear transformation zone model for amorphous solids, *Phys. Rev. E*, *76*(5), 056106.

Marone, C. (1998), Laboratory-derived friction laws and their application to seismic faulting, *Ann. Rev. Earth Planet. Sci.*, *26*, 643-696.

Morgan, J. K., and M. S. Boettcher (1999), Numerical simulations of granular shear zones using the distinct element method - 1. Shear zone kinematics and the micromechanics of localization, *J. Geophys. Res.*, *104*(B2), 2703-2720, doi:10.1029/1998JB900056.

Nielsen, S. B., J. M. Carlson, and K. B. Olsen (2000), Influence of friction and fault geometry on earthquake rupture, *J. Geophys. Res.*, *105*(B3), 6069-6088, doi:10.1029/1999JB900350.

Ono, I. K., C. S. O'Hern, D. J. Durian, S. A. Langer, A. J. Liu, and S. R. Nagel (2002), Effective temperature of a driven system near jamming, *Phys. Rev. Lett.*, *89*, 095703.

Perrin, G., J. R. Rice, and G. Zheng (1995), Self-healing slip pulse on a frictional surface, *J. Mech. Phys. Solids*, *43*, 1461-1495.

Rice, J. R. (2006), Heating and weakening of faults during earthquake slip, *J. Geophys. Res.*, *111*, B05311, doi:10.1029/2005JB004006.

Rosakis, A. J., O. Samudrala, and D. Coker (1999), Cracks faster than the shear wave speed, *Science*, *284*, 1337-1340, doi:10.1126/science.284.5418.1337.

Rudnicki, J. W., and J. R. Rice (1975), Conditions for the localization of deformation in pressure-sensitive dilatant materials, *J. Mech. Phys. Sol.*, *23*, 371-394.

Ruina, A. L. (1980), Friction laws and instabilities: A quasistatic analysis of some dry frictional behavior, Ph.D. Thesis, Brown University, Providence, R.I.

Schröter, M., D. I. Goldman, and H. L. Swinney (2005), Stationary state volume fluctuations in a granular medium, *Phys. Rev. E*, *71*, 030301.

Shi, Y., M. B. Katz, H. Li, and M. L. Falk (2007), Evaluation of the disorder temperature and free-volume formalisms via simulations of shear banding in amorphous solids, *Phys. Rev. Lett.*, *98*, 185505.

Templeton, E. L., and J. R. Rice (2008), Off-fault plasticity and earthquake rupture dynamics: 1. Dry materials or neglect of fluid pressure changes, *J. Geophys. Res.*, *113*, B09306, doi:10.1029/2007JB005529.

Tordesillas, A., J. F. Peters, and B. S. Gardiner (2004), Shear band evolution and accumulated microstructural development in Cosserat media, *Int. J. Numer. Anal. Methods Geomech.*, *28*, 981-1010, doi:10.1002/nag.343.

Tullis, T. E., and D. L. Goldsby (2003), Flash melting of crustal rocks at almost seismic slip rates, *Eos Trans. AGU*, *84*(46), Fall Meet. Suppl., Abstract S51B-05.

Wibberley, C. A. J., and T. Shimamoto (2003), Internal structure and permeability of major strick-slip fault zones: The Median Tectonic Line in Mie Prefecture, southwest Japan, *J. Struct. Geol.*, *25*(1), 59-78, doi:10.1016/S0191-8141(02)00014-7.

Zheng, G., and J. R. Rice (1998), Conditions under which velocity-weakening friction allows a self-healing versus a crack-like mode of rupture, *Bull. Seismol. Soc. Am.*, *88*, 1466-1483.

J. M. Carlson, E. G. Daub, Physics Department, Broida Hall, University of California, Santa Barbara, CA 93106, USA. (edaub@physics.ucsb.edu)

M. L. Manning, Princeton Center for Theoretical Science, 411B Jadwin Hall, Princeton, NJ, 08544, USA